Xiang et al. BMC Plant Biology (2019) 19:383
https://doi.org/10.1186/s12870-019-1990-9

BMC Plant Biology

RESEARCH ARTICLE Open Access

Transcriptomic and phosphoproteomic profiling and metabolite analyses reveal the mechanism of $NaHCO_3$-induced organic acid secretion in grapevine roots

Guangqing Xiang, Wanyun Ma, Shiwei Gao, Zhongxin Jin, Qianyu Yue and Yuxin Yao*

Abstract

Background: Organic acid secretion is a widespread physiological response of plants to alkalinity. However, the characteristics and underlying mechanism of the alkali-induced secretion of organic acids are poorly understood.

Results: Oxalate was the main organic acid synthesized and secreted in grapevine (a hybrid of *Vitis amurensis*, *V. berlandieri* and *V. riparia*) roots, while acetate synthesis and malate secretion were also promoted under $NaHCO_3$ stress. $NaHCO_3$ stress enhanced the H^+ efflux rate of grapevine roots, which is related to the plasma membrane H^+-ATPase activity. Transcriptomic profiling revealed that carbohydrate metabolism was the most significantly altered biological process under $NaHCO_3$ stress; a total of seven genes related to organic acid metabolism were significantly altered, including two phosphoenolpyruvate carboxylases and phosphoenolpyruvate carboxylase kinases. Additionally, the expression levels of five *ATP-binding cassette transporters*, particularly *ATP-binding cassette B19*, and two *Al-activated malate transporter 2 s* were substantially upregulated by $NaHCO_3$ stress. Phosphoproteomic profiling demonstrated that the altered phosphoproteins were primarily related to binding, catalytic activity and transporter activity in the context of their molecular functions. The phosphorylation levels of phosphoenolpyruvate carboxylase 3, two plasma membrane H^+-ATPases 4 and ATP-binding cassette B19 and pleiotropic drug resistance 12 were significantly increased. Additionally, the inhibition of ethylene synthesis and perception completely blocked $NaHCO_3$-induced organic acid secretion, while the inhibition of indoleacetic acid synthesis reduced $NaHCO_3$-induced organic acid secretion.

Conclusions: Our results demonstrated that oxalate was the main organic acid produced under alkali stress and revealed the necessity of ethylene in mediating organic acid secretion. Additionally, we further identified several candidate genes and phosphoproteins responsible for organic acid metabolism and secretion.

Keywords: Grapevine, Transcriptome, Phosphoproteome, Organic acid secretion, Alkali stress

Background

Soil alkalinity is an important environmental problem, and alkali stress primarily caused by $NaHCO_3$ and Na_2CO_3 severely affects crop growth and development in more than 434 million hectares of land worldwide [1]. Compared with neutral salt stress, alkali stress not only causes osmotic stress and ion injury but also leads to high pH injury [2, 3]; therefore, alkali stress is more destructive than salt stress [4]. However, in contrast to the extensive studies on plant salt tolerance, much less attention has been focused on exploring the mechanisms underlying alkali stress tolerance.

Under alkali stress, plants must regulate intracellular pH and the pH outside roots to maintain root functions. Organic acids play a key role in regulating the cell and rhizosphere pH levels. It was reported that organic acid metabolism is closely correlated with alkali stress tolerance [4]. *Puccinellia tenuiflora* roots accumulate and secrete citric acid into the rhizosphere in response to alkali stress [5]. HCO_3^- induces the production of

* Correspondence: yaoyx@sdau.edu.cn
State Key Laboratory of Crop Biology, Collaborative Innovation Center of Fruit & Vegetable Quality and Efficient Production, College of Horticulture Science and Engineering, Shandong Agricultural University, Tai-An 271018, Shandong, China

malate, succinate, and citrate in rice roots [6] and malate in maize roots [7]. Additionally, organic acids have been reported to function in plant adaptation to other abiotic stresses. For example, cotton and alfalfa accumulate more citric acid under drought and salt stresses, respectively [8, 9]. Plants accumulate organic acids in cells and secrete them into rhizospheres when facing Al, P and Cd toxicity [10–12]. With regard to the mechanisms of alkali-induced organic acid synthesis and secretion, some key enzymes involved in organic acid metabolism, such as citrate synthase, malate synthase and isocitrate lyase, have been suggested to determine alkali stress tolerance [13]. Plasma membrane H^+-ATPases, such as *Arabidopsis* AHA2 and AHA7, are necessary for proton secretion for plant tolerance to alkali stress [11, 14]. Additionally, some studies have demonstrated that ethylene and auxin have roles in the regulation of root H^+ secretion and alkali stress by regulating H^+-ATPase [15, 16].

To date, the pathways of organic acid metabolism in the cell and extrusion out of the cell under alkali stress remain largely unknown in grapevine. Genome-scale analysis of gene expression profiles is a powerful method to reveal plant abiotic stress tolerance mechanisms [17, 18]. For example, transcriptome profiling reveals the genetic basis of alkalinity tolerance in wheat [18] and gene networks responsive to $NaHCO_3$ stress in *Tamarix hispida* [17]. Quantitative and comprehensive insights into the mRNA transcriptome will contribute to unraveling the key mechanism of organic acid secretion in response to alkali treatment. On the other hand, phosphorylation represents one of the most important posttranslational modification functions in diverse biological pathways. The activities of several proteins related to organic acid synthesis and extrusion, such as phosphoenolpyruvate carboxylase (PEPC) and H^+-ATPase [19, 20], have been shown to be regulated by phosphorylation. An analysis of the comprehensive phosphorylation modifications induced by alkali stress is needed to better understand the process of organic acid secretion under alkali stress.

Grapevines are an economically important fruit crop worldwide that grow as deep-rooted perennial plants, and their growth and fruit quality are largely influenced by soil alkalinity and salinity. The majority of commercial rootstocks and varieties used in viticulture are moderately sensitive to alkali stress. However, the candidate rootstock cultivar A15 possesses strong alkali tolerance and is a suitable material for identifying alkali tolerance-associated genes. Additionally, A15 was identified to have an higher capacity to secrete organic acids than other grapevine rootstocks with moderate or weak tolerance to alkali stress [21]. The present study determined the accumulation and secretion of organic acids and H^+ efflux at different time points after $NaHCO_3$ treatment. Thereafter, the key genes and phosphoproteins involved in the above processes were identified using transcriptomic and phosphoproteomic analyses. Additionally, the roles of ethylene and indoleacetic acid (IAA) in mediating organic acid secretion under alkali conditions were evaluated. The results provide valuable information for dissecting the metabolism and regulatory pathways of alkali stress tolerance in grapevine roots.

Results

Effects of $NaHCO_3$ on the synthesis and secretion of organic acids in grapevine roots

A total of six organic acids were identified, oxalate, malate, tartrate, succinate, citrate and acetate. Oxalate was the main organic acid and accounted for 69.5–71.3% of the sum of the six organic acids in the control roots. In contrast, the five other organic acids, particularly citrate, showed relatively low concentrations (Fig. 1a-f). Similar differences in organic acid concentrations were also found in the culture solution (Fig. 1g-l); therefore, oxalate was the main organic acid synthesized and secreted by grapevine roots. The content of oxalate in the $NaHCO_3$-treated roots was significantly enhanced from 3 to 24 h after treatment (HAT) and reached a maximum increase of 87.1% at 12 HAT compared to that in the control roots (Fig. 1a). The increased synthesis of oxalate promoted oxalate secretion and led to continuous accumulation in the culture solution; the oxalate content in the $NaHCO_3$ culture solution reached 1.56 times that of the control solution at 24 HAT (Fig. 1g). Additionally, $NaHCO_3$ treatment continuously significantly enhanced acetate synthesis but did not promote its secretion (Fig. 1f, l). In contrast, the other organic acids were generally not affected by $NaHCO_3$ treatment. However, notably, the content of malate in the culture solution containing $NaHCO_3$ was substantially increased at all time points (Fig. 1h). On the other hand, NaCl treatment as a positive control produced different effects on organic acid synthesis and secretion, e.g., NaCl imparted a reduced and stronger influence on oxalate and malate secretion, respectively, than $NaHCO_3$ (Fig. 1g, h). Therefore, the changes in organic acid synthesis and secretion under $NaHCO_3$ were attributed to both Na^+ and $^-HCO_3$.

$NaHCO_3$ treatment promotes H^+ secretion of grapevine roots

To detect root H^+ secretion, the vine roots with different treatments were placed in solid medium with pH-sensitive bromocresol purple for 10 h (Fig. 2). Color changes occurred around the roots to indicate changes in pH. For the control roots, only less acidic substances were secreted, as indicated by the weak yellow color, at 0.5 and 3 days after treatment (DAT), and the acidic substances were gradually secreted and accumulated, generating a clear yellow color in the small area around the roots at 5

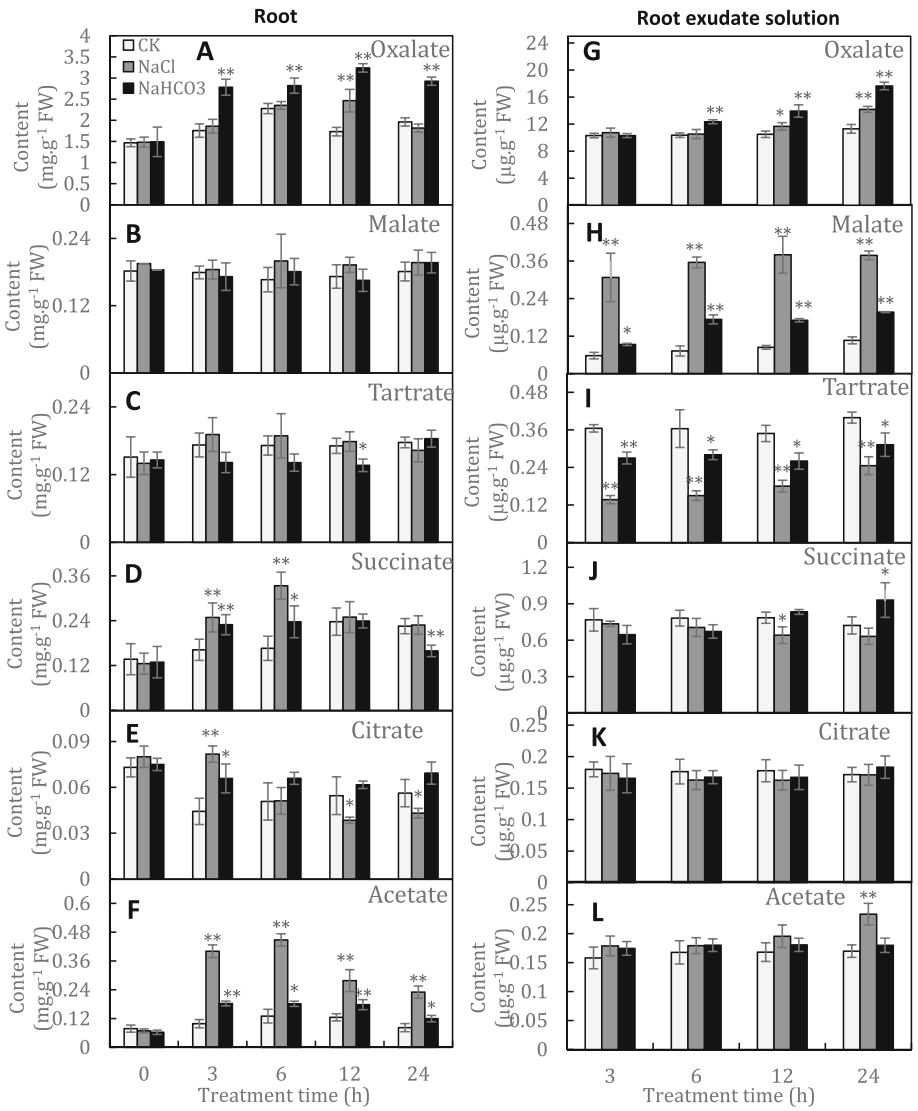

Fig. 1 The organic acid content in grapevine roots (**a**-**f**) and their culture solution (**g**-**l**) under nonstress, salt-stress and alkali-stress conditions. The organic acid content in the root exudate solution was expressed using the ratio of the content of organic acids in the root exudate solution to the root weight to reflect root secretion capacity. Values represent the means ± SD of three replicates. * Significant difference, $P < 0.05$; ** highly significant difference, $P < 0.01$

DAT (Fig. 2a). In contrast, the roots treated with $NaHCO_3$ began to produce a clear yellow color at 0.5 DAT and produced large areas of yellow color at 3 and 5 DAT (Fig. 2c), indicating that large amounts of acidic substances had accumulated. Additionally, the NaCl treatment as a positive control led to a clear yellow color, but the area and intensity were smaller than those under $NaHCO_3$ treatment (Fig. 2b, c); therefore, the production of acidic substances was attributed to both Na^+ and $^-HCO_3$. Moreover, the H^+-ATPase inhibitor Na_3VO_4 almost completely inhibited the production of yellow color (Fig. 2d), suggesting that acid secretion is related to the PM H^+-ATPase activity. Notably, the production of yellow color was accompanied by the occurrence of newly grown roots (Fig. 2a-c), and the production of yellow color and new roots was almost completely inhibited by the simultaneous treatment of $NaHCO_3$ plus Na_3VO_4 (Fig. 2d). Further experimentation using solid medium, half of which contained Na_3VO_4, indicated that root growth and H^+ secretion were substantially affected by H^+-ATPase activity (Fig. 2e). Therefore, $NaHCO_3$ treatment induced H^+ secretion, which was accompanied by new root growth.

On the other hand, H^+ flux was determined using noninvasive microtest technology to further determine H^+ secretion under $NaHCO_3$ treatment (Fig. 3a). High negative values of H^+ flux prior to treatment indicated the influx of H^+ into root cells. In contrast, the H^+ flux gradually changed to efflux, as indicated by the positive

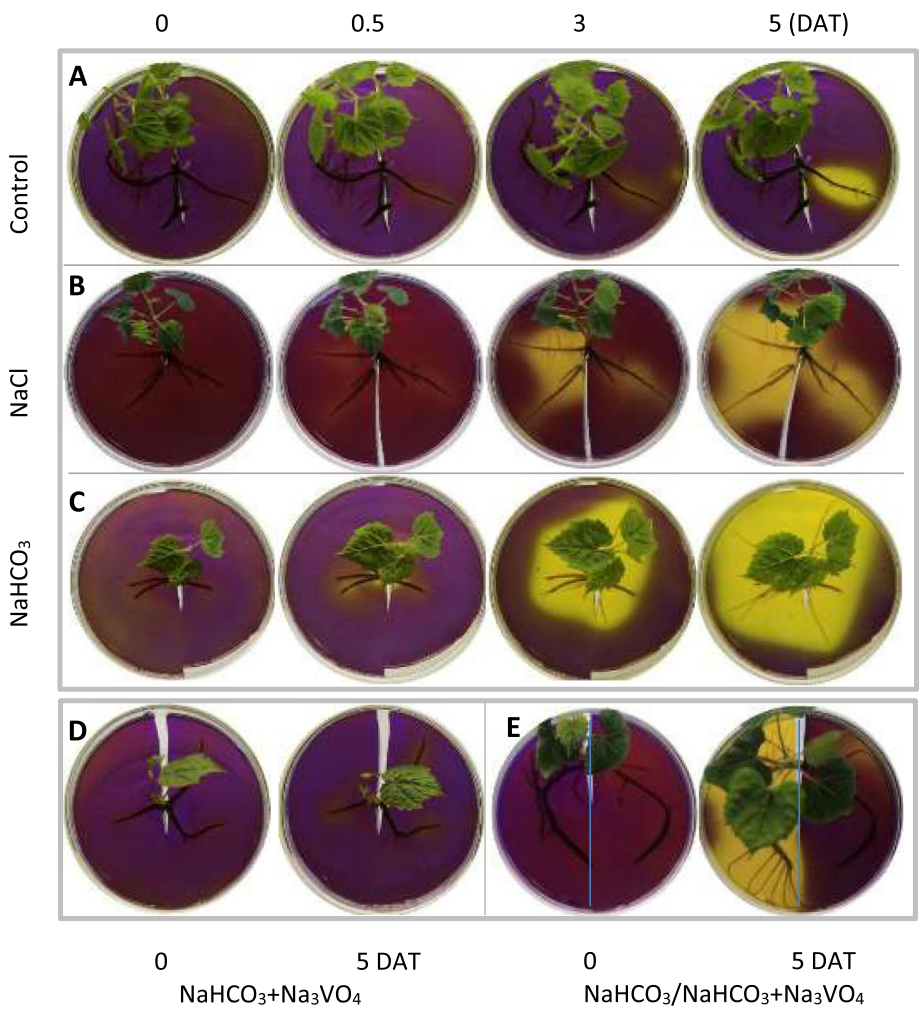

Fig. 2 Effects of $NaHCO_3$, NaCl and vanadate on rhizosphere acidification. The roots of five-week-old in vitro shoot cultures were treated with water (pH 7.0) (**a**), 75 mM NaCl (pH 7.0) (**b**), 75 mM $NaHCO_3$ (pH 8.7) (**c**), and 75 mM $NaHCO_3$ plus 0.1 mM Na_3VO_3 (**d**, **e**) for 6 h. After the roots were washed with deionized water, the roots were carefully spread on the bottom of a culture dish and then covered with an agar sheet containing 0.006% bromocresol purple and 0.8% agar. In addition to bromocresol purple and agar, Na_3VO_4 was added into the whole agar sheet in panel **d** and into the right side of the agar sheet in panel **e**

values in the control and $NaHCO_3$-treated roots from 1 HAT. Compared to the low H^+ efflux rate of the control roots, the H^+ efflux rate of the roots treated with $NaHCO_3$ was very high at 6 and 12 HAT. Additionally, the highest H^+ efflux rate in the treated roots occurred at 12 HAT. On the other hand, the $NaHCO_3$-treated roots possessed higher H^+-ATPase activity than the control roots, and the highest activity of the treated roots was found at 12 HAT, which was 0.46-fold higher than that in the control (Fig. 3b).

Identification of the changes in the transcriptome profile of grapevine roots in response to $NaHCO_3$

To explore the mechanism underlying the alkali stress-induced oxalate secretion, RNA-Seq analysis of the control and $NaHCO_3$-treated vine roots was conducted to quantify gene changes. A total of 3232 and 1714 genes were up- and downregulated by at least one-fold in the $NaHCO_3$-treated vine roots, respectively (Fig. 2), demonstrating that $NaHCO_3$ treatment caused massive transcriptional reprogramming in the vine roots. All of the annotated differentially expressed genes (DEGs) were associated with 20 biological processes. The process of carbohydrate metabolism contained the most DEGs; additionally, biosynthesis of other secondary metabolites, environmental adaptation, amino acid metabolism and signal transduction were also clearly changed biological processes (Fig. 4a).

In the carbohydrate metabolism process, the gene expression of seven genes involved in oxalate and malate metabolism was significantly altered by $NaHCO_3$ treatment (Fig. 2 and Fig. 4b). Two PEPCs and their kinases

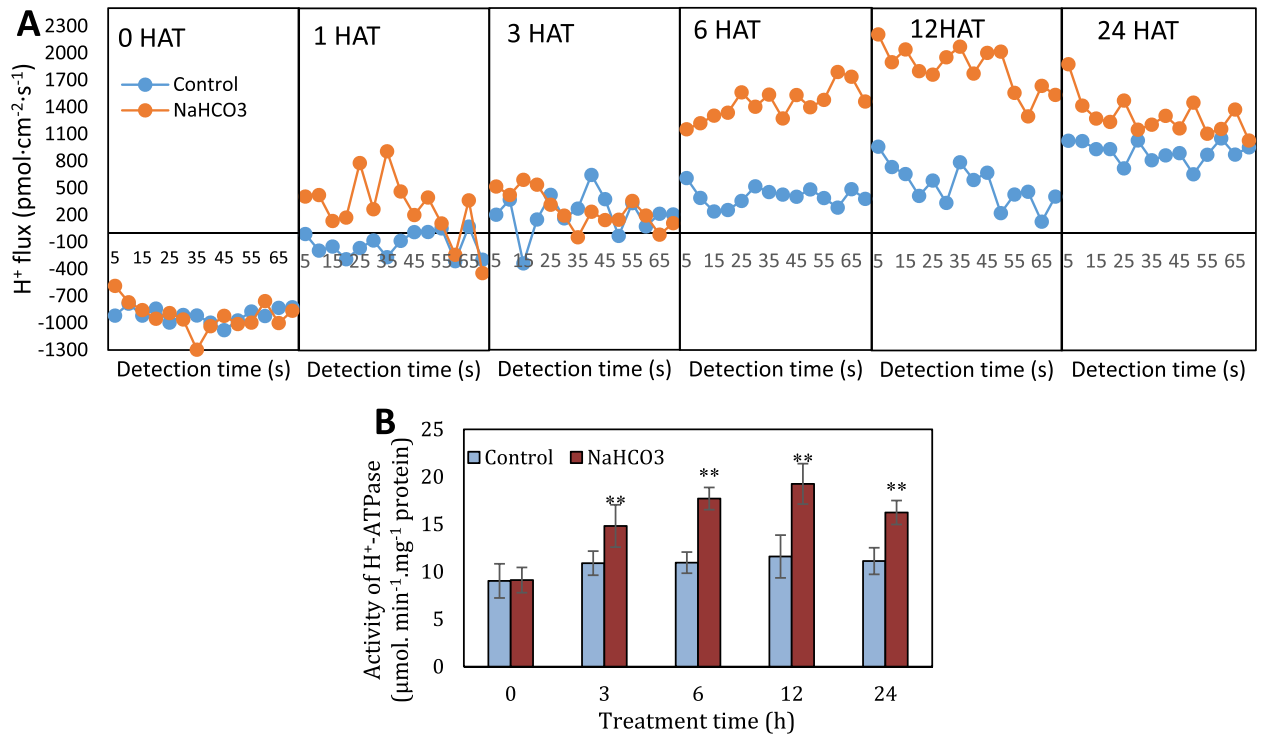

Fig. 3 H^+ flux (**a**) and H^+-ATPase activity (**b**) of root tips in response to $NaHCO_3$ treatment. Positive and negative values indicate the efflux and influx of H^+, respectively. Values are the means of three replicates, and error bars denote the SD. ** highly significant difference, $P < 0.01$

(PEPCKs) were significantly upregulated, positively contributing to the biosynthesis of oxaloacetate and thereby providing the substrate for oxalate and malate biosynthesis. An *oxalate--CoA ligase* gene (*OCL*) and two *NADP-malic enzyme* (ME) genes were significantly downregulated, which decreased the degradation of oxalate and malate, respectively. Additionally, the expression of five *ATP-binding cassette* (*ABC*) *transporters*, belonging to the process of membrane transport, was substantially increased, and in particular, the expression of *ATP-binding cassette B19* (*ABCB19*) increased 9.66-fold. Two *aluminum-activated malate transporters* (*ALMTs*) exhibited more than 5.0-fold higher expression in the $NaHCO_3$-treated roots than in the control roots. *Plasma membrane* (*PM*) *H^+-ATPases PMA2* and *AHA11* were only detected in the $NaHCO_3$-treated roots but showed very low values of reads per kilobase of transcript per million mapped reads (RPKM), suggesting that they might not be the primary proton pump in grapevine roots.

With respect to the signal transduction process, the most significantly altered pathway was the ethylene signaling pathway, for which 51 genes related to ethylene biosynthesis and signaling were transcriptionally modified. Six *1-aminocyclopropane-1-carboxylic acid* (*ACC*) *synthases* (*ACSs*) were substantially upregulated by $NaHCO_3$ treatment; in contrast, two *ACC oxidases* (*ACOs*) were transcriptionally changed, and *ACO1* was downregulated 2.97-fold (Additional file 1: Table S1). Additionally, IAA metabolism and signaling were also significantly changed. The expression of four genes related to IAA metabolism and signaling was upregulated more than 5-fold, including *indole-3-acetic acid-amido synthetase* (*GH3*) and three *IAA responsive factors* (*IAA12*, *SAUR32* and *SAUR40*). Moreover, six protein kinases located in the plasma membrane were substantially upregulated by $NaHCO_3$ treatment, suggesting that plasma membrane proteins were regulated by phosphorylation.

On the other hand, 34 differentially expressed genes, which contained genes involved in organic metabolism and transport and hormone biosynthesis and signaling, were detected by qRT-PCR at different times after $NaHCO_3$ treatment. Similar expression changes in the DEG tag profiles were found, which not only validated the reliability of the DEGs but also demonstrated their expression patterns under alkali stress (Fig. 4c).

Quantitative analysis of phosphoproteins with phosphorylation levels significantly changed in response to $NaHCO_3$

We identified 2669 unique phosphoproteins, collectively containing 6312 nonredundant phosphorylation sites. Among those phosphorylation sites, 5404 (85.6%) were found at serine, 877 (13.9%) were found at threonine

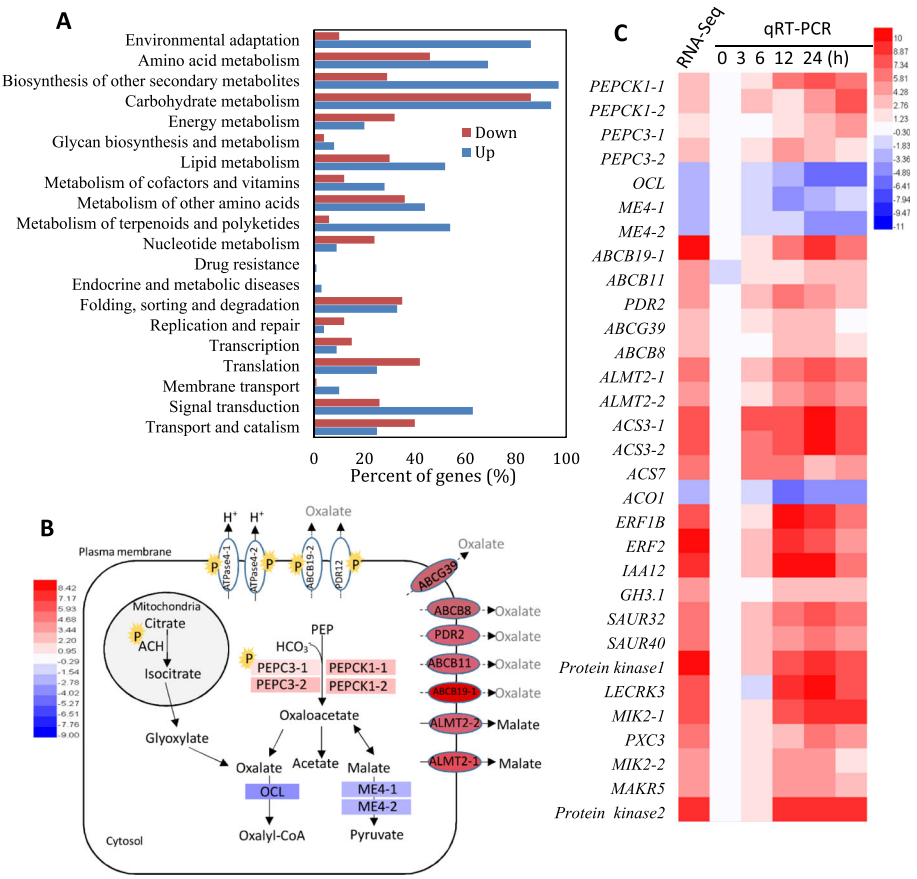

Fig. 4 Functional categories (**a**) of DEGs responding to alkali stress and the key genes and proteins involved in the metabolism and extrusion of organic acid (**b**, **c**) and signaling related to ethylene, IAA and receptor kinases (**c**). RNA-Seq was performed using the top 10-mm length of grapevine roots after 12 h of $NaHCO_3$ treatment. In panel **a**, functional categories of the DEGs from RNA-Seq were performed by Gene Ontology. In panel **b**, the schematic was constructed using the genes and proteins related to organic acid metabolism and extrusion. The normalized values of gene expression are shown on a color scale, and a P highlighted with a yellow background color denotes a phosphoprotein. The gray color indicates the possible transporters of oxalate. In panel **c**, the heatmap was constructed using the genes related to organic acid metabolism and transport, metabolism and signaling of ethylene and IAA, and receptor kinases. The normalized values of gene expression are shown on a color scale. Fold changes of qRT-PCR were calculated by comparing the relative expression values of the selected genes in the $NaHCO_3$-treated and control vine roots

and 31 (0.49%) were found at tyrosine residues. Of the 2669 phosphoproteins, 2141 phosphoproteins were identified, which contained different quantities of phosphorylation sites (from 1 to 25); a total of 1822 and 608 phosphoproteins contained one and two phosphorylation sites, respectively (Additional file 2: Table S2).

When comparing the phosphorylation levels between the $NaHCO_3$-treated and control samples, a total of 197 phosphoproteins (270 phosphorylation sites) showed a significant change (ratio ≥ 1.5, $P < 0.05$), with 107 upregulated and 163 downregulated (Additional file 2: Table S2). The 197 phosphoproteins were annotated using Blast2GO according to the biological process, cellular component and molecular function (Fig. 5a). The phosphoproteins were classified into 11 biological processes, with metabolic process, cellular process and localization as the top three categories. For the molecular function, phosphoproteins were classified into 9 categories, and the top 3 categories were binding, catalytic activity and transporter activity. For the cellular components, cell part, cell and membrane possessed the highest number of phosphoproteins (Fig. 5a). The phosphoproteins modified by $NaHCO_3$ were primarily localized in the nucleus, cytoplasm, chloroplast and plasma (Fig. 5b). Additionally, Motif-X analysis identified 16 significantly enriched motifs (Fig. 5c).

Aconitate hydratase (ACH) and PEPC3–1, which are involved in oxalate and malate synthesis, were significantly phosphorylated in the $NaHCO_3$ treatment compared to the control (Fig. 4b; Table 1). The phosphorylation levels of two plasma membrane-localized ATPases (ATPase4–1 and particularly ATPase4–2) were substantially enhanced, which are responsible for H^+ efflux and provide energy for the transport of oxalate and malate across the plasma

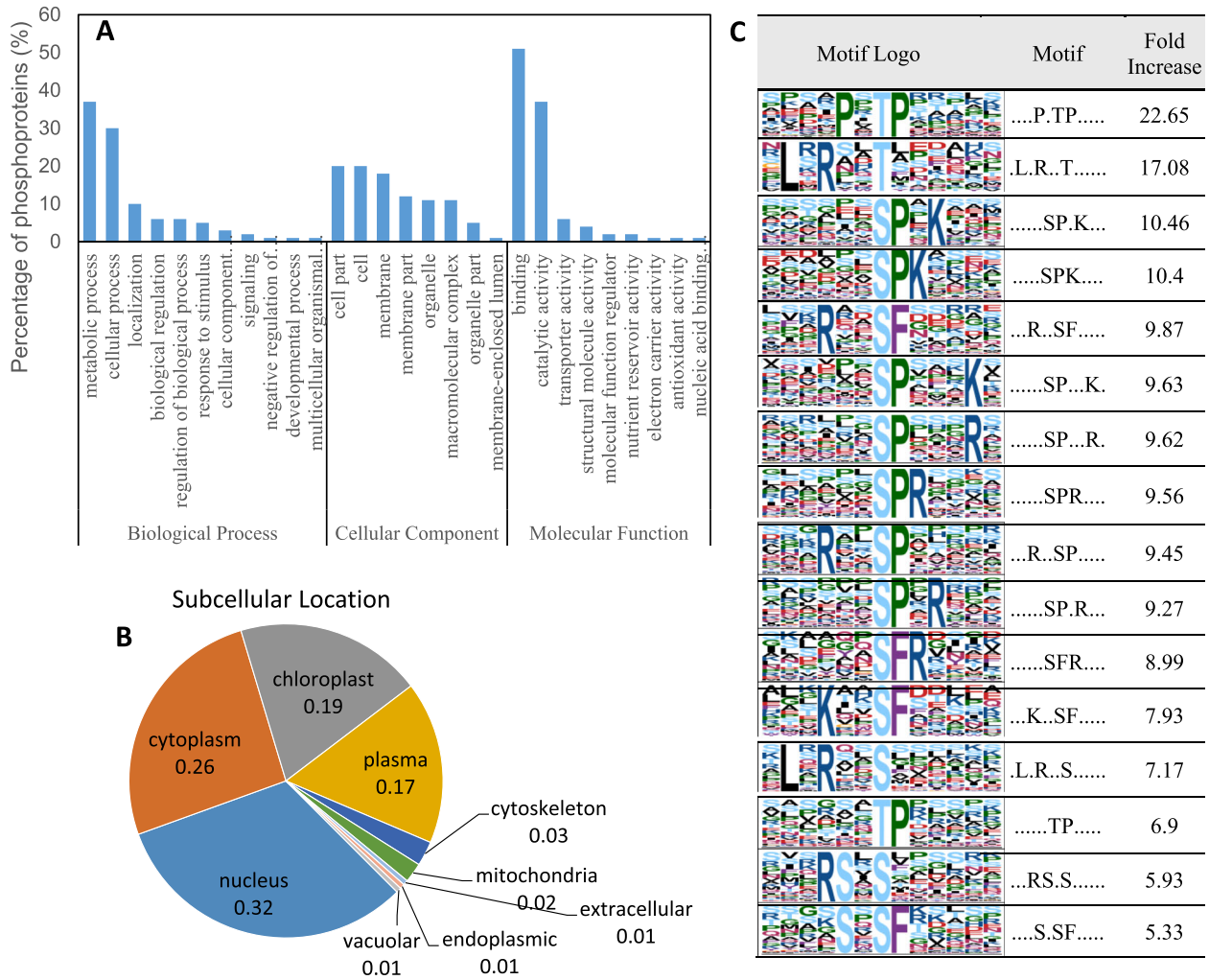

Fig. 5 The distribution of differentially phosphorylated proteins (**a**, **b**) and significantly enriched phosphorylated sites (**c**). The 197 phosphorylated proteins were classified according to their biological process, cellular component, molecular function and subcellular location (**a**, **b**). The Gene Ontology (GO) annotation proteome was derived from the UniProt-GOA database (www. http://www.ebi.ac.uk/GOA/). Soft motif-x was used to analyze the model of sequences constituted with amino acids in specific positions of modify-21-mers (10 amino acids upstream and downstream of the site, but phosphorylation with modified-13-mers was 6 amino acids upstream and downstream of the site) in all protein sequences. All of the database protein sequences were used as background database parameters and other parameters with default

membrane. Additionally, two plasma membrane ABC transporters ABCB19–2 and pleiotropic drug resistance 12 (PDR12), potential transporters of oxalate, were also significantly phosphorylated. Moreover, the phosphorylation levels of two plasma membrane-localized serine/threonine-protein kinases (STY46 isoform X1 and CDL1), ACO4 and ACO11 for ethylene synthesis and EIN2 for ethylene signaling were significantly changed (Fig. 4b; Table 1).

Organic acid secretion by vine roots involves ethylene and IAA

Transcriptomic and/or phosphoproteomic profiling indicated that the metabolism and signaling of IAA and ethylene were significantly altered by $NaHCO_3$ treatment. To reveal the role of ethylene and IAA in mediating $NaHCO_3$-induced organic acid secretion, the changes in ethylene and IAA under $NaHCO_3$ treatment and the effects of the inhibition of ethylene and IAA biosynthesis and/or signaling on organic acid secretion were determined. Compared with the control, $NaHCO_3$ treatment significantly increased ethylene production at 3 and 6 HAT but substantially decreased ethylene production at 12 and 24 DAT. In contrast, the IAA content was substantially reduced by $NaHCO_3$ at 6 DAT, and the decrease in the IAA content reached 57.6% at 24 HAT (Fig. 6a, b). Additionally, the inhibition of ethylene biosynthesis and perception via aminoethoxyvinylglycine (AVG) and 1-methylcyclopropene (1-MCP) completely blocked $NaHCO_3$-induced organic acid secretion, and the inhibition of IAA biosynthesis via 1-N-naphthylphthalamic acid

Table 1 Phosphorylation levels of the proteins involved in organic acid metabolism and transport and signaling in grapevine roots regulated by $NaHCO_3$ stress

Protein accession	Modified sequence (Probabilities)	Position	$NaHCO_3$/CK Ratio	*P* value	Protein description	Gene name	Subcellular Localization
D7T1R6	IIDWENS(0.244)S(0.756)PK	92	2.32	0.000522	ACH	VIT_00s0264g00030	mitochondria
F6H2N7	MAS(1)IDAQLR	11	1.74	0.0414	PEPC3–1	VIT_19s0014g01390	cytoplasm
D7SQD1	T(1)LHGLQPPETSNLFNDK	886	3.46	0.000023	ATPase 4–1	VIT_11s0052g00620	PM
D7SQD1	GLDIDTIQQHYT(1)V	953	2.43	0.00746	ATPase 4–1	VIT_11s0052g00620	PM
D7SQD1	GHVES(1)VVK	936	2.10	0.00126	ATPase 4–1	VIT_11s0052g00620	PM
D7SQD1	ELS(1)EIAEQAK	909	1.59	0.00464	ATPase 4–1	VIT_11s0052g00620	PM
F6H3A8	S(1)IGLEEIK	6	1.97	0.00178	ATPase 4–2	VIT_04s0008g02460	PM
F6H3A8	GHMES(1)VVK	936	1.94	0.000255	ATPase 4–2	VIT_04s0008g02460	PM
F6H3A8	T(1)LHGLQPPETSNIFSDK	886	1.62	0.00172	ATPase 4–2	VIT_04s0008g02460	PM
F6H3A8	GLDIDTIQHHYT(1)V	953	1.51	0.00762	ATPase 4–2	VIT_04s0008g02460	PM
F6H5R3	NLSYQY(0.002)S(0.953)T(0.045)GADGR	645	1.94	0.0407	ABCB19–2	VIT_14s0108g00430	PM
F6H5R3	LSHS(0.03)LS(0.964)T(0.006)K	626	1.85	0.004	ABCB19–2	VIT_14s0108g00430	PM
F6HX69	S(0.986)S(0.014)GADVFSR	22	1.86	0.0194	PDR 12	VIT_09s0002g05600	PM
F6HX69	S(0.933)S(0.067)RDEDDEEALK	31	1.56	0.000376	PDR12	VIT_09s0002g05600	PM
F6HFE2	GLVDS(0.996)GITTIPR	65	0.61	0.0059	ACO 4	VIT_01s0011g05650	chloroplast
F6HKN0	GLSDS(0.997)GIT(0.002)SIPR	28	0.59	0.0015	ACO 11	VIT_08s0007g03040	cytoskeleton
F6HR32	EISGSSPSLTSEGPGS(1)FR	648	1.66	0.0201	EIN 2	VIT_08s0040g01730	PM
D7U4Z3	QSWPNHHS(0.014)LS(0.976)PT(0.011)GEQEETGIK	266	1.55	0.0311	STY46 isoform X1	VIT_03s0038g03040	cytoplasm
F6HDG9	DGSSAQS(1)HHVTR	36	3.535	0.00204	CDL1	VIT_05s0020g01770	cytoplasm
F6HDG9	LGS(0.989)PS(0.01)T(0.001)HKNS(1)PDFR	420	1.955	0.0332	CDL1	VIT_05s0020g01770	cytoplasm
F6HDG9	LGS(0.989)PS(0.01)T(0.001)HKNS(1)PDFR	413	1.955	0.0332	CDL1	VIT_05s0020g01770	cytoplasm

PM Plasma membrane, *ACH* Aconitate hydratase, *PEPC* Phosphoenolpyruvate carboxylase, *CDL* Serine/threonine-protein kinase CDL, *ACO* 1-aminocyclopropane-1-carboxylate oxidase, *EIN2* Ethylene-insensitive protein 2. The values of the $NaHCO_3$/CK ratio are presented as the means of three replicates

(NPA) significantly reduced $NaHCO_3$-induced organic acid secretion (Fig. 6c, d). Therefore, ethylene signaling is necessary to regulate organic acid secretion under $NaHCO_3$, and IAA also participates in the process; additionally, their roles are largely affected by their concentrations in plants.

Discussion

Accumulation and secretion of oxalate are important physiological responses of grapevine roots to alkali stress

Plant roots are in direct contact with the soil and can adjust to an adverse rhizosphere environment by secreting a large amount of compounds, which is the

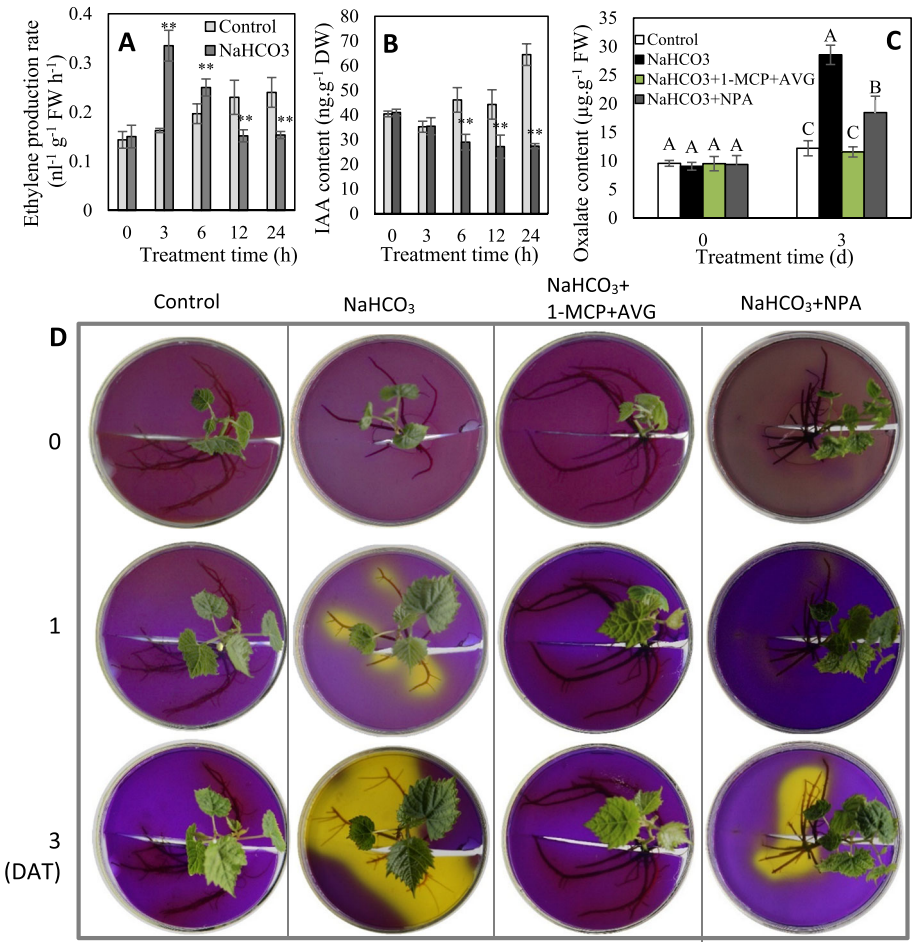

Fig. 6 Changes in ethylene (**a**) and IAA (**b**) and the effects of their inhibition on organic acid secretion (**c**, **d**). 1-MCP, 1-methylcyclopropene, an inhibitor of ethylene perception; AVG, 1-N-naphthylphthalamic acid, an inhibitor of IAA transport; and AVG, aminoethoxyvinylglycine, an inhibitor of ethylene biosynthesis. DAT, days after treatment. In panels **a**-**c**, values represent the means ± SD of three replicates. ** highly significant difference, $P < 0.01$; values indicated by different capital letters are significant at $P < 0.01$ at the same treatment time

most direct and obvious response of roots to environmental stresses [5]. Under alkali stress, the accumulation of organic acids is observed in many plants. Oxalate was highly accumulated and secreted by grapevine roots under alkali stress (Fig. 1a, g). A large amount of oxalate was also found in the roots of *Kochia sieversiana* and *Suaeda glauca* under alkali stress [22, 23]. In contrast, *Chloris virgata* was found to predominantly accumulate citrate, and wheat roots secrete large amounts of lactic, acetic and formic acids under alkali stress [24, 25]. The accumulation and secretion of organic acids, including oxalate, citrate and malate, play important roles in osmoregulation, pH adjustment, and ionic balance maintenance by providing a negative charge under alkali and salt stresses [5, 22, 23]. This study demonstrated that both $NaHCO_3$ and NaCl stimulated the secretion of organic acids, but $NaHCO_3$ created a more acidic rhizosphere environment (Fig. 2b, c). Additionally, $NaHCO_3$ and NaCl imparted different effects on oxalate, acetate and malate (Fig. 1). Similarly, previous reports have also demonstrated that alkali and salt stress have different effects on organic acid metabolism and secretion. For example, the concentration of citrate, the most dominant organic acid, is substantially increased by alkali stress but decreased by salt stress in *Puccinellia tenuiflora* roots; additionally, alkali stress causes the secretion of citric acid into the rhizosphere, while salt stress does not [5]. Different changes in citrate and malate were also found in *Chloris virgata* under alkali and salt stresses [25].

Therefore, organic acid secretion is a widespread physiological response of plants, but oxalate is the primary organic acid synthesized and secreted by vine roots. Additionally, $^{-}HCO_3$ plays a key role in inducing oxalate synthesis and secretion in grapevine roots.

The possible pathway of organic acid synthesis and secretion based on the key genes and phosphoproteins under alkali stress

Three pathways for oxalate biosynthesis have been proposed in plants, i.e., the glycolate/glyoxylate pathway, the ascorbate pathway and the oxaloacetate (OAA) pathway [26, 27]. Under alkali stress, substantial amounts of $^{-}HCO_3$ enter the root and provide the substrate for PEPCs, which catalyze the β-carboxylation of PEP to OAA using $^{-}HCO_3$ in the cytosol in an irreversible process [28]; thereafter, OAA can be converted to oxalate, acetate and malate (Fig. 4b). In *Arabidopsis*, the *pepc3* mutant abolished the salt stress-induced increase in malate, suggesting the role of *AtPEPC3* in regulating organic acid synthesis [29]. The significant upregulation of the expression of two *PEPC3* genes under alkali stress might enhance OAA synthesis and the subsequent conversion of OAA to oxalate and acetate (Fig. 4b, c). In addition to transcriptional regulation, PEPC activity is also regulated by phosphorylation catalyzed by phosphoenolpyruvate carboxylase kinase (PEPCK) [20]. PEPC phosphorylation is abolished in the *pepc3* mutant of *Arabidopsis* under salt stress [20], suggesting that PEPC3 might be the target protein of PEPCKs. The significant increases in the expression levels of two *PEPCK1* genes and the phosphorylation level of PEPC3–1 also suggested the phosphorylation regulation of PEPC3–1 by PEPCK1s (Fig. 4b, c). Collectively, the above results suggest that the OAA pathway is the main pathway for oxalate and acetate biosynthesis under alkali stress. However, notably, the glycolate/glyoxylate pathway might also be modified in grapevine roots under alkali stress, as indicated by the significant increase in the phosphorylation level of aconitate hydratase (aconitase), a key protein in the glycolate/glyoxylate pathway [30].

H^+ extrusion and the transport of organic acid anions across the plasma membrane are controlled by PM H^+-ATPases, providing energy by creating an electrochemical proton gradient for transporters [31]. The PM H^+-ATPase is important for the root proton-secretion adaptation to alkaline stress [15]; high PM H^+-ATPase activity and proton secretion have been shown to enhance plant tolerance to alkaline stress [32], while lower PM H^+-ATPase activity and proton secretion result in sensitity to alkaline stress [33]. PM H^+-ATPase activity is tightly regulated by phosphorylation at several N- and C-terminal residues, especially upon exposure to various environmental stimuli [34]. The significant increase in the phosphorylation levels showed that the two ATPases 4 are the key proton pumps in grapevine roots under alkali stress (Fig. 4b, Table 1). The ATPases 4 from *Arabidopsis* (AHA4) and tobacco (PMA4) plants are also reported to be involved in salt tolerance [35, 36]. Therefore, ATPase 4 might function in plant tolerance to alkali and salt stress.

In contrast, the specific transporter of oxalate remains unclear. Nevertheless, some experiments have indicated the role of ABC transporters in transporting organic acids in plants. Four ABC transporters (ABCG11, ABCG21, ABCA2, and ABCB21) were considered to be potentially involved in oxalate and/or citrate secretion under Al stress in *Grain amaranth* roots [10]. AtPDR6, belonging to the ABCG subfamily of the ABC transporter family, is involved in the root extrusion of organic acids, including succinate, fumarate and malate [37]. In this study, the expression levels of five *ABC transporter*s, particularly *ABCB19–1*, were substantially increased by $NaHCO_3$ treatment (Fig. 4b, Additional file 1: Table S1), suggesting their association with organic acid secretion. In particular, the expression of *ABCB19–1* was well correlated with the oxalate content in roots (Fig. 4c, Fig. 1a), suggesting its role in transporting oxalate. Additionally, two ABC transporters, ABCB19–2 and PDR12, were significantly phosphorylated (Table 1), and PDR12 has been reported to mediate the extrusion of water-soluble carboxylate anions in yeast [38]; therefore, ABCB19–2 and PDR12 might participate in the transport of organic acids. However, the detailed function of the above transporters must be characterized in future studies.

ALMTs are found throughout plant genomes and are involved in a range of distinct functions in different cell types. ALMT1 functions in mediating organic acid secretion in the Al-tolerance response in many plant species [39]. In contrast, the ALMT2 transporter mediates an Al-independent electrogenic transport of organic anions, such as malate and citrate, across the plasma membrane in wheat [40]. The upregulation of two *ALMT2s* (Fig. 4b, c) and the increased content of malate implied that ALMT2 transporters mediate the salt- and alkali-induced malate extrusion in vine roots. Notably, a large increase in malate secretion was not accompanied by its accumulation under salt and alkali stress (Fig. 1b, h). A similar phenomenon was also found in other plants under Al stress [22, 41]. Therefore, it is suggested that malate metabolism is not a limiting factor but rather that transporters are more important for its secretion under alkali stress.

The signaling pathway mediating alkali stress-induced organic acid secretion

Ethylene is an important signaling molecule mediating numerous important biological processes, including responses to abiotic stresses [42]. In this study, the application of inhibitors related to ethylene biosynthesis and perception indicated the necessity of ethylene in organic acid secretion under alkaline stress (Fig. 6c, d). However, the exogenous application or endogenous overproduction of ethylene substantially inhibited H^+-ATPase activity and H^+ efflux in rice roots under alkali stress [17]; additionally, ethylene production was reduced with $NaHCO_3$ treatment (Fig. 6a). Similarly, transgenic tobacco plants with poor ethylene

biosynthesis exhibited elevated salt tolerance, while rice plants treated with ethylene exhibited salt hypersensitivity [43, 44]. Therefore, the role of ethylene might be concentration-dependent [42, 45], and low-concentration ethylene might be necessary to mediate $NaHCO_3$-induced organic acid secretion. Ethylene biosynthesis is mainly regulated by ACS and ACO at the transcriptional and posttranslational levels [46, 47]. When grapevines were subjected to alkali stress, the decline in ethylene production was accompanied (Fig. 6a) by the decreased expression of *ACO1* (Fig. 4c) and phosphorylation levels of ACO4 and ACO11 (Table 1) but the increased expression of *ACS3* and *ACS7* (Fig. 4c), suggesting the key role of ACOs in regulating ethylene synthesis under alkali stress. Additionally, EIN2, a central regulator of ethylene signaling [48], controls the transduction of the ethylene signal from the ER membrane to the nucleus in *Arabidopsis* [48], and its phosphorylation inhibited ethylene signaling (Table 1; 48). After the signal cascade mediated by EIN5, EIN6, EIN3 and others, ethylene signals are delivered to ethylene responsive factors (ERFs), the last downstream components of the ethylene signaling pathway, which lead to the regulation of ethylene controlled gene expression [43]. Here, the changes in the expression of a large amount of ERFs may correspond to the different biological processes regulated by ethylene under alkali stress.

Auxin has been reported to control root apoplastic acidification, to enhance the Al-induced exudation of citrate and to promote the phosphorylation of PM H^+-ATPases [13, 45, 49]. Additionally, PIN2 (an auxin efflux transporter) activates plasma membrane H^+-ATPases to release protons, which is necessary for the adaptation of *Arabidopsis* to alkali stress [15]. Therefore, auxin plays a key role in regulating organic acid secretion under alkali stress. A recent study found that endogenous auxin controls apoplastic acidification; however, an endogenous increase in the overexpression of auxin biosynthesis gene or exogenous increase in the auxin level induces a transient alkalinization [45], which is similar to the role of ethylene discussed above. Here, $NaHCO_3$ treatment induced a decrease in IAA, but NPA treatment reduced organic acid secretion (Fig. 6b-d), suggesting that the fine-tuning of IAA biosynthesis may be essential for the regulation of organic acid secretion. Additionally, the genes of *IAA12* and *GH3* as IAA repressors [45, 50] were also substantially upregulated (Fig. 4c), probably reducing IAA synthesis and signaling. Small auxin-up RNA (SAUR) genes represent the largest family of auxin-responsive genes and participate in auxin-mediated PM H^+-ATPase activation [45, 51]. The large increase in the expression of *SAUR32* and *SAUR40* suggests that they likely regulate organic acid secretion in response to auxin in vine roots. Particularly, it has been demonstrated that auxin mediates ethylene signaling to control root growth [52]. Therefore, we inferred that ethylene most likely regulates organic acid secretion through auxin signaling in vine roots under alkali stress.

On the other hand, the cell membrane harbors hundreds of different receptor kinases that receive environmental signals at the receptor domain on the extracellular side of the membrane and convert these signals into cellular responses via an intracellular protein kinase domain [34]. The PM H^+-ATPase was reported to interact with multiple such receptor kinases [53]. The receptor kinase-mediated control of primary active proton pumping at the plasma membrane, e.g., PSY1R, increases proton efflux from roots by interacting with and phosphorylating AHA2/AHA1 [54]. In this study, the high-level expression and/or phosphorylation of the 11 plasma membrane-located receptor kinases might participate in the regulation of ATPases. Although the exact roles of candidate genes remain to be examined, our data provide a platform for further functional analyses of these genes.

Conclusion

Oxalate was the primary organic acid synthesized and secreted by vine roots under $NaHCO_3$ stress. The OAA pathway, including two PEPC3s and PEPCK1s, plays a key role in oxalate synthesis. The secretion of organic acids and H^+ were controlled by PM H^+-ATPases, and two phosphorylated PM ATPases 4 were the main proton pumps under $NaHCO_3$ stress. Additionally, ABCB19–2 and PDR12 might participate in the transport of oxalate and other organic acids. Low-concentration ethylene mediates $NaHCO_3$-induced organic acid secretion, and IAA also participates in this process.

Methods

Determination of organic acids in grapevine roots and root exudate solutions

Healthy apical growth tips of A15 vines were removed in early summer to establish grapevine in vitro shoot cultures. The shoot cultures were subcultured on Murashige and Skoog medium containing 3% (w/v) sucrose, 7 g. L^{-1} agar and 0.2 mg. L^{-1} IBA. Five-week-old grapevine in vitro shoot cultures were transferred to glass bottles with a 10-cm height and 5-cm diameter. The vines were treated with 50 ml water (pH 7.0) as a control, 75 mM NaCl (pH 7.0) and $NaHCO_3$ (pH 8.7). Each glass bottle was provided sufficient oxygen with an oxygen machine (SenSen Group, China). The vines were grown in a controlled-environment growth cabinet at 25 °C, a 16-h photoperiod and a light intensity of 600 μmol/m^2/s. At different time points after different treatments, the roots were collected and immediately frozen in liquid nitrogen for organic acid extraction. The treatment

solution was collected and evaporated to dryness with a rotary evaporator, and the residue was dissolved in 1 ml double distilled water. The filtrate, which was passed through a 0.45-μm filter, was used for organic acid determination. The extraction of organic acids from the roots and their determination for root extract and treatment solutions were performed using a capillary electrophoresis system (Beckman P/ACE, Palo Alto, CA) as described in our previous study [55].

H^+ secretion test

H^+ secretion was detected according to a previously described method [56]. Five-week-old grapevine A15 in vitro shoot cultures were treated with water (pH 7.0), 75 mM NaCl (pH 7.0), 75 mM $NaHCO_3$ (pH 8.7), and 75 mM $NaHCO_3$ plus 0.1 mM Na_3VO_3 for 6 h. Then, the roots were rinsed, carefully spread in Petri dishes and covered by solid medium (pH 5.8) which consisted of 0.006% bromocresol purple (pH indicator, discoloration range of 5.2–6.8), 1 mmol l^{-1} $CaSO_4$, 2.5 mmol l^{-1} K_2SO_4 and 0.8% agar. The vines were grown in a controlled-environment growth cabinet at 25 °C and continuous illumination at 400 μmol/m^2/s light intensity.

Measurement of H^+-ATPase activity and H^+ flux in roots

Plant materials were the same as those described in the organic acid determination Section. The extraction of plasma membrane (PM) protein and activity determinations of PM H^+-ATPase of the root tips were conducted according to the method of Yan et al. (2002) [56]. The activity of H^+-ATPase was determined by the Pi amount after 30 min of reaction in 0.5 ml of 30 mM BTP/MES buffer (pH 6.5), 5 mM $MgSO_4$, 50 mM KCl, 1 mM Na_2MoO_4, 1 mM NaN_3, 5 mM ATP, and Brij 58 (0.02% w/v). The reaction was initiated by adding 5 mg of membrane protein and stopped with 1 ml of stopping reagent (2% H_2SO_4, 5% SDS, and 0.7% $(NH_4)_2MoO_4$) followed immediately by the addition of 50 μl ascorbic acid (10% w/v). The color development was completed after 30 min. The absorbance at 820 nm was measured using a spectrophotometer.

Root H^+ fluxes were measured using the scanning ion-selective electrode technique with a Noninvasive Microtest Technology System (NMT, Xuyue Beijing Sci. & Tech. Co., Ltd., Beijing, China). The 10-mm long roots from the root apex were equilibrated in the measurement solution for 20 min and then immobilized in the measurement chamber in 5 ml of fresh measuring solution.

RNA-Seq and quantitative real-time PCR (qRT-PCR)

Total RNA of 10-mm-long grapevine roots from the apex was extracted using TRIzol Reagent (Invitrogen, Carlsbad, CA, USA), and mRNA was isolated using poly-T oligo attached magnetic beads. Transcriptome sequencing and analysis were conducted by OE Biotech Co., Ltd. (Shanghai, China). Sequencing libraries, constructed using NEBNext® Ultra™ RNA Library Prep Kit for Illumina® (7530 L, NEB, United States), were sequenced on an Illumina HiSeq 4000 platform, and 150-bp paired-end reads were generated. Clean reads were assembled into transcripts using Cufflinks referencing the grape genome (http://genomes.cribi.unipd.it/grape/). The unigene expression levels were quantified using RPKM. Unigenes that were differentially expressed between two samples were screened using a false discovery rate < 0.05 and absolute $\log_2$ (fold change) ≥1 as the threshold. Three biological replicates were generated for the control and $NaHCO_3$ treatment.

qRT-PCR was performed using SYBR Green Master-Mix (SYBR Premix EX Taq TM, Dalian, China) on a Bio-Rad iQ5 (Hercules, CA, United States) instrument, and the primers are listed in Additional file 3: Table S3.

Phosphopeptide and phosphoprotein identification and quantification

Proteins from grapevines were extracted and quantified with the BCA kit (Beyotime, Beijing, China). After trypsin digestion, the peptide mixture was desalted on a Strata X C_{18} SPE column (Phenomenex, Torrance, CA, USA). Each peptide was vacuum-dried and reconstituted in 0.5 M TEAB (Sigma, USA). The peptide mixture was labeled using TMT kit (Thermo Fisher Scientific, Torrance, CA, USA) according to the manufacturer's introduction. The TMT labeled peptides were fractionated by high pH reverse-phase HPLC and concentrated by vacuum centrifugation. The phosphopeptides were enriched using IMAC microspheres, and they were then eluted with elution buffer, followed by lyophilization and LC-MS/MS analysis. The phosphopeptides were dissolved in 0.1% formic acid (solvent A) and loaded onto a C_{18}-reversed phase column (15-cm length, 75 μm i.d., packed in-house) and separated with a linear gradient of solvent B (0.1% formic acid in 98% acetonitrile) at a constant flow rate of 0.4 μL/min on an EASY-nLC 1000 UPLC system (Thermo). The peptides were eluted with a gradient of 6 to 23% solvent B for 26 min, 23 to 35% solvent B for 8 min, and 80% solvent B for 6 min. The peptides were detected and identified by tandem mass spectrometry (MS/MS) in Q ExactiveTM Plus (Thermo) coupled online to the UPLC, which was supported by Jingjie PTM BioLabs (Hangzhou, China). MS/MS data were searched using a Maxquant search engine (v1.5.2.8) against the *Vitis vinifera* proteome concatenated with reverse decoy database. The parameters in Maxquant searches were as follows: max missing cleavage of Trypsin/P, 2; peptide mass tolerance, 20 ppm in the first search and 5 ppm in the main search; MS/MS tolerance, 0.02 Da; fixed modification, carbamidomethyl on

Cys; variable modification, oxidations on Met. FDR was adjusted to < 1%.

IAA extraction and determination

IAA extractions were performed according to our previous study [57]. Separation and quantification of IAA were carried out using a Scientific Ultimate 3000 HPLC system (Thermo, San Jose, CA, USA) coupled to a TSQ Quantum Access MAX system (Thermo, San Jose, CA, USA). HPLC separation was performed using a Thermo Scientific Hypersil Gold column (50 × 2.1 mm, 1.9 μm). The injection volume was 10 μL. The mobile phase consisted of 0.5% acetic acid in water (A) and methanol (B) with the following gradient at a flow rate of 1.0 $ml.min^{-1}$: 0–0.5 min, 0–20% B; 0.5–3.0 min, 20–90% B; 3.0–6.5 min, 90% B; 6.5–10.0 min, 90–20% B; 10.0–15.0 min, 20% B. Detection and quantification of IAA were performed using the ESI negative mode. The parameters were set as follows: parent mass by charge (m/z) of 263.1, daughter mass by charge (m/z) of 153.0, and a collision energy of 14 eV.

Determination of the ethylene production rate

The ethylene production rate was measured using a GC-9A gas chromatograph (Shimadzu, Japan) equipped with a GDX-502 column and a flame ionization detector. The vine roots were enclosed in a 5-mL centrifuge tube with sealing film and incubated at 25 °C for 3 h. Five milliliters of the headspace gas was withdrawn from each tube through the septum stopper using a gas-tight syringe and assayed.

Statistical analyses

Statistical analysis was performed with the SPSS (V19.0) statistical software package. A one-way analysis of variance followed by Duncan's multiple range test was employed.

Additional files

Additional file 1: Table S1. RNA-Seq profiles of the control and $NaHCO_3$-treated vine roots. Unigenes differentially expressed between two samples were screened using a false discovery rate < 0.05 and absolute $\log_2$ (fold changes) ≥ 1 as the threshold. (XLSX 1337 kb)

Additional file 2: Table S2. Analysis of phosphopeptide changes in grapevine roots exposed to $NaHCO_3$ stress. The significantly altered phosphoproteins between two samples were screened using fold changes ≥1.5 or ≤ 0.67 ($P < 0.05$). (XLSX 96 kb)

Additional file 3: Table S3. Primer sequences for real-time quantitative RT-PCR. Gene ID is derived from the grape genome (http://genomes.cribi.unipd.it/grape/). (DOCX 17 kb)

Abbreviations

1-MCP: 1-methylcyclopropene; ABCB19: ATP-binding cassette B19; ACC: 1-aminocyclopropane-1-carboxylic acid; ACH: Aconitate hydratase; ACO: 1-aminocyclopropane-1-carboxylic acid oxidase; ACS: 1-aminocyclopropane-1-carboxylic acid synthase; ALMT: Aluminum-activated malate transporter; AVG: Aminoethoxyvinylglycine; DAT: Days after treatment; DEG: Differentially expressed gene; HAT: Hours after treatment; IAA: Indoleacetic acid; ME: Malic enzyme; NPA: 1-N-naphthylphthalamic acid; OCL: Oxalate-CoA ligase; PDR12: Pleiotropic drug resistance 12; PEPC: Phosphoenolpyruvate carboxylase; PEPCK: PEPC kinase; PM: Plasma membrane; qRT-PCR: quantitative real-time PCR; RPKM: Reads per kilobase of transcript per million mapped reads

Acknowledgments

Not applicable.

Authors' contributions

YY and GX conceived and designed the research; GX, WM and SG performed the experiments; ZJ and QY analyzed the data; and YY wrote the manuscript. All authors read and approved the manuscript.

Funding

This study was financially supported by the National Natural Science Foundation of China (31872068), the National Key Research and Development Program (2018YFD1000200), the Funds of Shandong "Double Tops" Program (SYL2017YSTD10) and China's Agricultural Research System (CARS-29). None of the funding bodies have any role in the design of the study or collection, analysis, and interpretation of data as well as in writing the manuscript.

Availability of data and materials

The mass spectrometry proteomics data have been deposited to the ProteomeXchange Consortium via the PRIDE partner repository with the dataset identifier PXD013746 (http://www.ebi.ac.uk/pride). Full RNA-Seq data were submitted to the sequence read archive (SRA) of NCBI under BioSample accessions SAMN11579694 and SAMN11579695 (https://www.ncbi.nlm.nih.gov/sra).

Ethics approval and consent to participate

Not applicable.

Consent for publication

Not applicable.

Competing interests

The authors declare that they have no competing interests.

Received: 22 May 2019 Accepted: 27 August 2019
Published online: 03 September 2019

References

1. Jin H, Plaha P, Park JY, Hong C, Lee IS, Yang Z, et al. Comparative EST profiles of leaf and root of *Leymus chinensis*, a xerophilous grass adapted to high pH sodic soil. Plant Sci. 2006;170:1081–6.
2. Gong B, Wen D, Bloszies S, Li X, Wei M, Yang F, et al. Comparative effects of NaCl and $NaHCO_3$ stresses on respiratory metabolism, antioxidant system, nutritional status, and organic acid metabolism in tomato roots. Acta Physiol Plant. 2014;36:2167–81.
3. Yang C, Shi D, Wang D. Comparative effects of salt and alkali stresses on growth, osmotic adjustment and ionic balance of an alkali-resistant halophyte *Suaeda glauca* (Bge.). Plant Growth Regul. 2008;56:179–90.
4. Shi D, Sheng Y. Effect of various salt–alkaline mixed stress conditions on sunflower seedlings and analysis of their stress factors. Environ J Exp Bot. 2005;54:8–21.
5. Guo L, Shi D, Wang D. The key physiological response to alkali stress by the alkali-resistant halophyte *Puccinellia tenuiflora* is the accumulation of large quantities of organic acids and into the rhyzosphere. J Agron Crop Sci. 2010;196:123–35.
6. Yang X, Römheld V, Marschner H. Effect of bicarbonate on root growth and accumulation of organic acids in Zn-inefficient and Zn-efficient rice cultivars (*Oryza sativa* L.). Plant Soil. 1994;164:1–7.
7. Alhendawi RA, Römheld V, Kirkby EA, Marschner H. Influence of increasing bicarbonate concentrations on plant growth, organic acid accumulation in roots and iron uptake by barley, sorghum, and maize. J Plant Nutr. 1997;20:1731–53.

8. Timpa JD, Burke JJ, Quisenberry JE, Wendt CW. Effects of water stress on the organic acid and carbohydrate compositions of cotton plants. Plant Physiol. 1986;82:724–8.
9. Fougère F, Le Rudulier D, Streeter JG. Effects of salt stress on amino acid, organic acid and carbohydrate composition of root, bactericide and cymosely of alfalfa (*Medicago sativa* L.). Plant Physiol. 1991;96:1228–36.
10. Fan W, Xu J, Lou H, Xiao C, Chen W, Yang J. Physiological and molecular analysis of aluminium-induced organic acid anion secretion from grain amaranth (*Amaranthus hypochondriacus* L.) roots. Int J Mol Sci. 2016;17:608.
11. Yuan W, Zhang D, Song T, Xu FY, Lin S, Xu W, et al. *Arabidopsis* plasma membrane H^+-ATPase genes AHA2 and AHA7 have distinct and overlapping roles in the modulation of root tip H^+ efflux in response to low-phosphorus stress. J Exp Bot. 2017;68:1731–41.
12. Tao Q, Hou D, Yang X, Li T. Oxalate secretion from the root apex of *Sedum alfredii* contributes to hyperaccumulation of cd. Plant Soil. 2016;398:139–52.
13. Wang P, Yu W, Zhang J, Rengel Z, Xu J, Han Q, et al. Auxin enhances aluminium-induced citrate exudation through upregulation of *GmMATE* and activation of the plasma membrane H^+-ATPase in soybean roots. Ann Bot. 2016;118:933–40.
14. Liu J, Guo Y. The alkaline tolerance in *Arabidopsis* requires stabilizing microfilament partially through inactivation of PKS5 kinase. J Genet Genomics. 2011;38:307–13.
15. Xu W, Jia L, Baluška F, Ding G, Shi W, Ye N, Zhang J. PIN2 is required for the adaptation of *Arabidopsis* roots to alkaline stress by modulating proton secretion. J Exp Bot. 2012;63:6105–14.
16. Chen H, Zhang Q, Cai H, Xu F. Ethylene mediates alkaline-induced rice growth inhibition by negatively regulating plasma membrane H^+-ATPase activity in roots. Front Plant Sci. 2017;8:1839.
17. Wang C, Gao C, Wang L, Zheng L, Yang C, Wang Y. Comprehensive transcriptional profiling of $NaHCO_3$-stressed *Tamarix hispida* roots reveals networks of responsive genes. Plant Mol Biol. 2014;84:145–57.
18. Meng C, Quan TY, Li ZY, Cui KL, Yan L, Liang Y, et al. Transcriptome profiling reveals the genetic basis of alkalinity tolerance in wheat. BMC Genomics. 2017;18:24.
19. Chen Q, Kan Q, Wang P, Yu W, Yu Y, Zhao Y, et al. Phosphorylation and Interaction with the 14–3-3 Protein of the plasma membrane H+-ATPase are involved in the regulation of magnesium-mediated increases in aluminum-induced citrate exudation in broad bean (*Vicia faba* L.). Plant Cell Physiol. 2015;56:1144–53.
20. Boxall SF, Dever LV, Knerová J, Gould PD, Hartwell J. Phosphorylation of phosphoenolpyruvate carboxylase is essential for maximal and sustained dark CO_2 fixation and core circadian clock operation in the obligate crassulacean acid metabolism species *Kalanchoë fedtschenkoi*. Plant Cell. 2017;29:2519–36.
21. Guo S, Niu Y, Zhai H, Han N, Du Y. Effects of alkaline stress on organic acid metabolism in roots of grape hybrid rootstocks. Sci Hortic. 2018;227:255–60.
22. Ma J, Ryan PR, Delhaize E. Aluminium tolerance in plants and the complexing role of organic acids. Trends Plant Sci. 2001;6:273–8.
23. Yang C, Wang P, Li C, Shi D, Wang D. Comparison of effects of salt and alkali stresses on the growth and photosynthesis of wheat. Photosynthetica. 2008;46:107–14.
24. Yang G. Alkali stress induced the accumulation and secretion of organic acids in wheat. Afr J Agric Res. 2012;7:2844–52.
25. Wang H, Bai B, Bai Z, Shi L, Ye J, Fan S, et al. Enzymatic regulation of organic acid metabolism in an alkali-tolerant halophyte *Chloris virgata* during response to salt and alkali stresses. Afr J Biotechnol. 2016;15:2243–50.
26. Franceschi VR, Nakata PA. Calcium oxalate in plants: formation and function. Annu Rev Plant Biol. 2005;56:41–71.
27. Yu L, Jiang J, Zhang C, Jiang L, Ye N, Lu Y, et al. Glyoxylate rather than ascorbate is an efficient precursor for oxalate biosynthesis in rice. J Exp Bot. 2010;61:1625–34.
28. Poschenrieder C, Fernández JA, Rubio L, Pérez L, Terés J, Barceló J. Transport and use of bicarbonate in plants: current knowledge and challenges ahead. Int J Mol Sci. 2018;19:1352.
29. Feria AB, Bosch N, Sánchez A, Nieto-Ingelmo AI, Osa CD, Echevarría C, et al. Phosphoenolpyruvate carboxylase (PEPC) and PEPC-kinase (PEPC-k) isoenzymes in *Arabidopsis thaliana*: role in control and abiotic stress conditions. Planta. 2016;244:901–13.
30. Coleman Z, Boelter K, Espinosa AS, Goggi RG, Palmer D, Sandhu D. Isolation and characterization of the aconitate hydratase 4 (*Aco4*) gene from soybean. Can J Plant Sci. 2017;97:684–91.
31. Morsomme P, Boutry M. The plant plasma membrane H^+-ATPase: structure, function and regulation. Biochim Biophys Acta Biomembr. 2000;1465:1–16.
32. Fuglsang AT, Guo Y, Cuin TA, Qiu Q, Song C, Kristiansen KA, et al. *Arabidopsis* protein kinase PKS5 inhibits the plasma membrane H^+-ATPase by preventing interaction with 14-3-3 protein. Plant Cell. 2007;19:1617–34.
33. Yang Q, Qin Y, Xie C, Zhao F, Zhao J, Liu D, et al. The *Arabidopsis* chaperone J3 regulates the plasma membrane H^+-ATPase through interaction with the PKS5 kinase. Plant Cell. 2010;22:1313–32.
34. Falhof J, Pedersen JT, Fuglsang AT, Palmgren M. Plasma membrane H^+-ATPase regulation in the center of plant physiology. Mol Plant. 2016;9:323–37.
35. Vitart V, Baxter I, Doerner P, Harper JF. Evidence for a role in growth and salt resistance of a plasma membrane H^+-ATPase in the root endodermis. Plant J. 2001;27:191–201.
36. Gévaudant F, Duby G, Stedingk EV, Zhao R, Morsomme P, Boutry M. Expression of a constitutively activated plasma membrane H^+-ATPase alters plant development and increases salt tolerance. Plant Physiol. 2007;144:1763–76.
37. Badri DV, Loyola-Vargas VM, Broeckling CD, De-la-Peña C, Jasinski M, Sanelia D, et al. Altered profile of secondary metabolites in the root exudates of *Arabidopsis* ATP-binding cassette transporter mutants. Plant Physiol. 2008; 146:762–71.
38. Piper P, Mahé Y, Thompson S, Pandjaitan R, Holyoak C, Egner R, et al. The Pdr12 ABC transporter is required for the development of weak organic acid resistance in yeast. EMBO J. 1998;17:4257–65.
39. Sharma T, Dreyer I, Kochian L, Piñeros MA. The ALMT family of organic acid transporters in plants and their involvement in detoxification and nutrient security. Front Plant Sci. 2016;7:1488.
40. Ligaba A, Maron L, Shaff J, Kochian L, Piñeros M. Maize ZmALMT2 is a root anion transporter that mediates constitutive root malate efflux. Plant Cell Environ. 2012;35:1185–200.
41. Yokosho K, Yamaji N, Ma J. Global transcriptome analysis of Al-induced genes in an Al-accumulating species, common buckwheat (*Fagopyrum esculentum* Moench). Plant Cell Physiol. 2014;55:2077–91.
42. Zhang M, Smith JAC, Harberd NP, Jiang C. The regulatory roles of ethylene and reactive oxygen species (ROS) in plant salt stress responses. Plant Mol Biol. 2016;91:651–9.
43. Müller M, Munné-Bosch S. Ethylene response factors: a key regulatory hub in hormone and stress signaling. Plant Physiol. 2015;169:32–41.
44. Yang C, Ma B, He SJ, Xiong Q, Duan K, Yin C, et al. MAOHUZI6/ETHYLENE INSENSITIVE3-LIKE1 and ETHYLENE INSENSITIVE3-LIKE2 regulate ethylene response of roots and coleoptiles and negatively affect salt tolerance in rice. Plant Physiol. 2015;169:148–65.
45. Barbez E, Dünser K, Gaidora A, Lendl T, Busch W. Auxin steers root cell expansion via apoplastic pH regulation in *Arabidopsis thaliana*. PNAS. 2017; 114:4884–93.
46. Argueso CT, Hansen M, Kieber JJ. Regulation of ethylene biosynthesis. J Plant Growth Regul. 2007;26:92–105.
47. Lyzenga WJ, Booth JK, Stone SL. The *Arabidopsis* RING-type E3 ligase XBAT32 mediates the proteasomal degradation of the ethylene biosynthetic enzyme, 1-aminocyclopropane-1-carboxylate synthase 7. Plant J. 2012;71:23–34.
48. Ju C, Yoon GM, Shemansky JM, Lin D, Ying Z, Chang J, et al. CTR1 phosphorylates the central regulator EIN2 to control ethylene hormone signaling from the ER membrane to the nucleus in *Arabidopsis*. PNAS. 2012; 109:19486–91.
49. Takahashi K, Hayashi K, Kinoshita T. Auxin activates the plasma membrane H^+-ATPase by phosphorylation during hypocotyl elongation in *Arabidopsis*. Plant Physiol. 2012;159:632–41.
50. Peat TS, Böttcher C, Newman J, Lucent D, Cowieson N, Davies C. Crystal structure of an indole-3-acetic acid amido synthetase from grapevine involved in auxin homeostasis. Plant Cell. 2012;24:4525–38.
51. Spartz AK, Ren H, Park MY, Grandt KN, Lee SH, Murphy AS, et al. SAUR inhibition of PP2C-D phosphatases activates plasma membrane H^+-ATPases to promote cell expansion in *Arabidopsis*. Plant Cell. 2014;26: 2129–42.
52. Li J, Xu H, Liu W, Zhang X, Lu Y. Ethylene inhibits root elongation during alkaline stress through AUXIN1 and associated changes in AUXIN accumulation. Plant Physiol. 2015;168:1777–91.
53. Ladwig F, Dahlke RI, Stührwohldt N, Hartmann J, Harter K, Sauter M. Phytosulfokine regulates growth in *Arabidopsis* through a response module at the plasma membrane that includes CYCLIC NUCLEOTIDE-GATED CHAN NEL17, H^+-ATPase, and BAK1. Plant Cell. 2015;27:1718–29.

54. Fuglsang AT, Kristensen A, Cuin TA, Schulze WX, Persson J, Thuesen KH, et al. Receptor kinase-mediated control of primary active proton pumping at the plasma membrane. Plant J. 2014;80:951–64.
55. Yao Y, Li M, Liu Z, Hao Y, Zhai H. A novel gene, screened by cDNA-AFLP approach, contributes to lowering the acidity of fruit in apple. Plant Physiol Biochem. 2007;45:139–45.
56. Yan F, Zhu Y, Müller C, Zörb C, Schubert S. Adaptation of H^+-pumping and plasma membrane H^+-ATPase activity in proteoid roots of white lupin under phosphate deficiency. Plant Physiol. 2002;129:50–63.
57. Xu L, Yue Q, Xiang G, Bian F, Yao Y. Melatonin promotes ripening of grape berry via increasing the levels of ABA, H_2O_2 and particularly ethylene. Hortic Res. 2018;5:41.

Publisher's Note